# Energy transfer of highly vibrationally excited azulene. III. Collisions between azulene and argon

Chen-Lin Liu,[a] Hsu Chen Hsu,[b] Jia-Jia Lyu,[c] and Chi-Kung Ni[a),d]
*Institute of Atomic and Molecular Sciences, Academia Sinica, P.O. Box 23-166, Taipei 10617, Taiwan*

(Received 14 August 2006; accepted 12 October 2006; published online 28 November 2006)

The energy transfer dynamics between highly vibrationally excited azulene molecules (37 582 $cm^{-1}$ internal energy) and Ar atoms in a series of collision energies (200, 492, 747, and 983 $cm^{-1}$) was studied using a crossed-beam apparatus along with time-sliced velocity map ion imaging techniques. The angular resolved collisional energy-transfer probability distribution functions were measured directly from the scattering results of highly vibrationally excited azulene. Direct *T-V/R* energy transfer was found to be quite efficient. In some instances, nearly all of the translational energy is transferred to vibrational/rotational energy. On the other hand, only a small fraction of vibrational energy is converted to translational energy (*V-T*). Significant amount of energy transfer from vibration to translation was observed at large collision energies in backward and sideway directions. The ratios of total cross sections between *T-V/R* and *V-T* increases as collision energy increases. Formation of azulene-argon complexes during the collision was observed at low enough collision energies. The complexes make only minor contributions to the measured translational to vibrational/rotational (*T-V/R*) energy transfer. © *2006 American Institute of Physics*.
[DOI: 10.1063/1.2388267]

## I. INTRODUCTION

The collisional deactivation of molecules containing chemically significant amounts of energy has been studied for several decades. In the early gas-phase experiments, energy transfer efficiency was obtained from the collisional quenching of activated molecules and unimolecular rate coefficients in the low-pressure and falloff regions.[1] Studies concerning the pressure dependence of unimolecular reaction rates have revealed that most collisions are far less efficient than strong collisions.

Recently new experimental techniques have been developed in order to understand fundamental energy transfer properties of highly vibrationally excited polyatomic molecules.[2,3] In these studies, highly vibrationally excited molecules are prepared by optical excitation to the electronic excited state, followed by the rapid internal conversion to the ground electronic state. The collisional deactivation of the highly vibrationally excited molecules with the bath cold molecules is then probed using various techniques. For examples, infrared fluorescence[4–12] and UV transient absorption[13–25] were used to probe the collisional deactivation of these molecules. Average energy transferred $\langle \Delta E \rangle$ per collision and its dependence on the internal energy $E$ of the high energy molecules were obtained from these techniques. An alternate approach to investigate the energy loss from the energetic molecules is to focus on the energy gain in the energy-accepting collision partners. Scattering data from the state-selective energy gain were fitted to an empirical model in order to estimate the average transferred energy.[26–34] Another interesting experiment is the chemical activation through vibrational energy transfer from highly vibrationally excited molecules.[35–37] The probability of $\Delta E$, which $\Delta E$ is larger than chemical activation energy, can be found experimentally. Large amount of energy transfer (>11 700 $cm^{-1}$) was observed from these experiments. Recently, kinetically controlled selective ionization (KCSI) method allows for a more sensitive probing of the collisional processes.[38–40] This technique can selectively ionize the deactivated molecules from a predetermined range of window (width is about 2000 $cm^{-1}$) within a quasicontinuum of rovibrational states. The parameters of a given functional form of energy transfer distribution $P(E',E)$ are then determined by averaging all possible initial $E$ and final $E'$ through a fitting procedure.

In our previous studies, we demonstrated the generation of a pure highly vibrationally excited azulene beam[41] and the usage of this azulene beam in the crossed-beam study.[42,43] Recent trajectory calculations under the identical initial conditions show that there is a broad agreement between experiment and computation.[44,45] In this work, we extend the study to the collisions between highly vibrationally excited azulene and argon. Angular resolved energy transfer distribution functions were obtained directly from the scattered highly vibrationally excited azulene. Comparison to the collisions of azulene and Kr atom is made.

## II. EXPERIMENT

The experimental details have been described in previous study.[43] Only a brief description is given here. The ex-

[a)]Also at Department of Chemistry, National Tsing Hua University, Hsinchu 30013, Taiwan.
[b)]Also at Department of Chemistry, National Taiwan University, Taipei 10617, Taiwan.
[c)]Also at Department of Chemistry, National Taiwan Normal University, Taipei, Taiwan.
[d)]Author to whom correspondence should be addressed. Electronic mail: ckni@po.iams.sinica.edu.tw

 

perimental apparatus includes two pulsed laser sets at 266 and 157 nm, a differentially pumped crossed molecular beam vacuum chamber and a time-of-flight mass spectrometer (TOF-MS) with a time-sliced velocity-map ion imaging system. The Az/rare gas mixtures were expanded through a pulsed nozzle to form the molecular beam. Carrier gases included ultrapure (99.999%) Ne, Ar, or mixtures of Ne (66%) and He (34%) at total pressures of 50–70 psi for the different collision energies. An Ar atom beam was created in the other source chamber by expanding ultrapure Ar (99.999%) at a pressure of 200 psi through a pulsed nozzle. Both the molecular beam and the Ar atom beam were positioned perpendicular to the time-of-flight axis of the mass spectrometer. The two beams crossed each other at two different fixed angles, 25° and 60°. The crossing point is 4 mm below the center of the ion optics.

A pulsed UV laser set at 266 nm crossed the azulene molecular beam 16 mm upstream from the crossing point of the atomic and molecular beams. Hot azulene was produced after absorbing a single 266 nm photon. Absorption of a 266 nm photon corresponds to excitation to the $S_4$ excited state. The absorption cross section is very large and it can easily be saturated. The fluorescence quantum yield from the excited state is very small ($<2\%$) and internal conversion to the ground electronic state dominates,[46] About 73% of the cold azulene molecules absorbed a single UV photon in their transformation to hot azulene. Approximately 19% of cold azulene molecules absorbed multiple UV photons. They either isomerized to naphthalene and then dissociated into fragments within few nanoseconds[47] or become cations which are deflected by electric field. Only 8% of the azulene molecules did not absorb any UV photon and remained as cold azulene in the molecular beam.[41] These cold molecules mainly distributed in the front part of the pulsed molecular beam, which was not irradiated by the UV laser beam.

After colliding with the Ar atom beam, azulene molecules were ionized by a 10 mm laser sheet at 157 nm. The kinetic energy and angular distributions of the scattered azulene molecules were measured by a TOF-MS that incorporates time-sliced velocity-map ion imaging techniques.[48,49] Unscattered azulene in the molecular beam were also photoionized by the 157 nm laser beam. Ions having the same velocity as the molecular beam were focused by the ion optics into a small spot on the micro-channel plate (MCP) detector. In order to avoid saturation and possible damage to the detector, a $2\times25$ mm$^2$ stainless steel pin located 5 cm in front of the detector was used to block these ions. As a result, part of the image at forward direction was obscured by the pin.

## III. RESULTS AND DATA ANALYSIS

In crossed-beam experiments, two beams cross each other on a time scale of at least several microseconds. Products with relatively high velocities in the laboratory frame tend to fly away from the detection zone during the crossing period, unlike slower moving products, which tend to accumulate and therefore have a higher probability of being ionized by a probe laser. A "density-to-flux" transformation is performed to calibrate the nonuniform detection sensitivity.[48] The details of density-to-flux matrix calculation have been described in previous study.[43] The sensitivity difference of different velocity products is smaller than a factor of 3. The small difference in each sensitivity matrix in our experiments is attributed to the large area crossed by the ionizing laser sheet. This significantly reduces the experimental uncertainty in the density-to-flux transformation. The low concentration of cold molecules remained in the molecular beam also reduces the experimental uncertainty from the background subtraction.

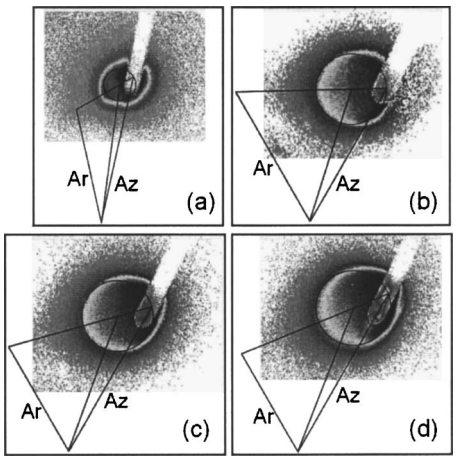


FIG. 1. Images and Newton diagrams for collision energies of (a) 200 cm$^{-1}$, (b) 492 cm$^{-1}$, (c) 747 cm$^{-1}$, and (d) 983 cm$^{-1}$.

Figure 1 shows the images of scattered hot azulene from collisions with Ar atoms at collision energies of 200, 492, 747, and 9830 cm$^{-1}$, respectively. The images have been calibrated by the sensitivity matrices and contribution from cold azulene has been subtracted. The calibration and subtraction procedures have been described in previous study.[43] Figure 1 also include the respective Newton diagrams, initial azulene and Ar beam velocities, center of mass velocity, relative velocity, and elastic collision circle. The elastic collisions are distributed on the elastic collision circle according to their deflection angles. The elastic collisions that have small deflection angles are obscured by the stainless pin and cannot be detected. The image inside the elastic collision circle corresponds to the decrease of the azulene velocity. It represents the energy up $\Delta E_{\mathrm{up}}$, translation to vibration/rotation ($T$-$V/R$) collisions. The image outside the elastic collision circle corresponds to the increase of the azulene velocity. It represents the energy down $\Delta E_{\mathrm{dn}}$, vibration to translation ($V$-$T$) collisions. All of these images (for the different collision energies) share a similar feature, a strong intensity distribution in the forward scattering direction. Additionally, there is a backward scattering peak with small intensity near the elastic collision circle at the lowest collision energy. Outside of the elastic collision circle, the intensity in the forward scattering direction decreases rapidly with increasing $\Delta E_{\mathrm{dn}}$. The backward scattering intensity is not as large and also does not decrease as fast as that for forward scattering.

The cross sections at different angles for both $T$ to $V/R$ and $V$ to $T$ energy transfer were obtained from sin $\theta$ multi-

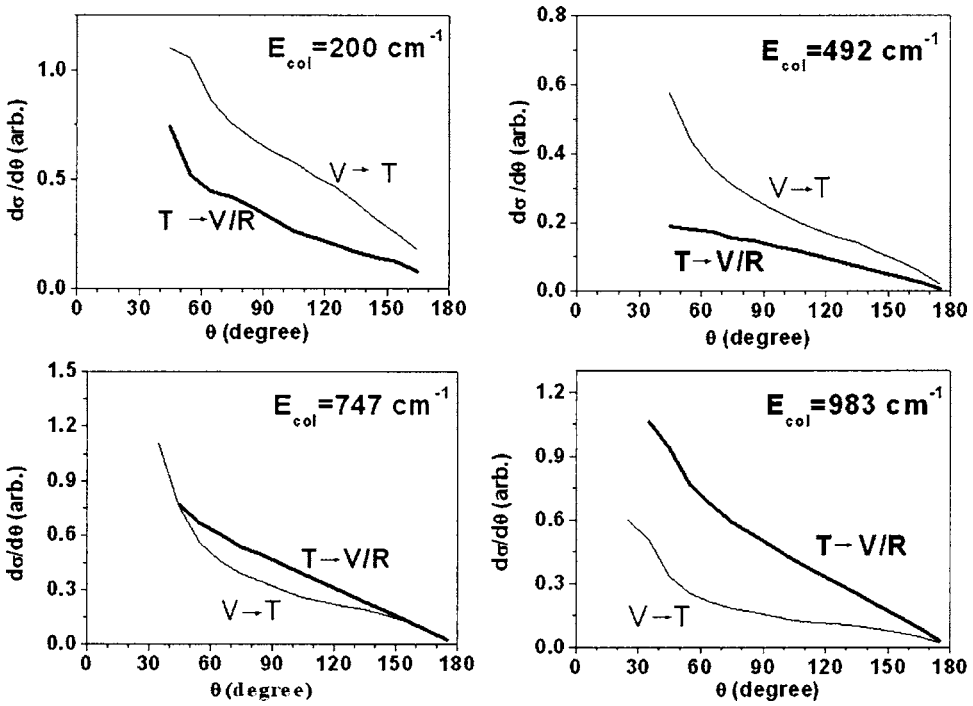


FIG. 2. Angular dependence of *T-V/R* and *V/T* cross sections at various collision energies.

plied by the integration of image intensity at very solid angle of $\pi^2/81$ s inside and outside the elastic circle, respectively. The results are shown in Fig. 2. In general, the cross section decreases as the deflection angle increases. However, the ratios of total cross sections between *T-V/R* and *V-T* increase as collision energy increases.

The energy-transfer probability distribution functions at various scattering angles are presented in Figs. 3 and 4. We noticed that molecular beam velocity distribution has effect on the energy-transfer probability distribution functions. Although the effect is small due to the large speed ratio $(V/\Delta V)$ of molecular beam, it is angle and collision-energy dependent. The energy-transfer probability distribution functions, illustrated in Figs. 3 and 4, show the shapes of energy-transfer probability density functions after the deconvolution from relative velocity distribution. The energy transfer probabilities for both energy down *V-T* and energy up *T-V/R* collisions are shown. For the energy down *V-T* collisions, the shapes of the energy transfer probabilities are nearly identical for forward, side, and backward scatterings at the lowest collision energy (200 $cm^{-1}$). Most of the transferred energy for the various scattering angles is less than 600 $cm^{-1}$. As the collision energy increases the shapes of the distribution functions for both sideway and backward scattering change.

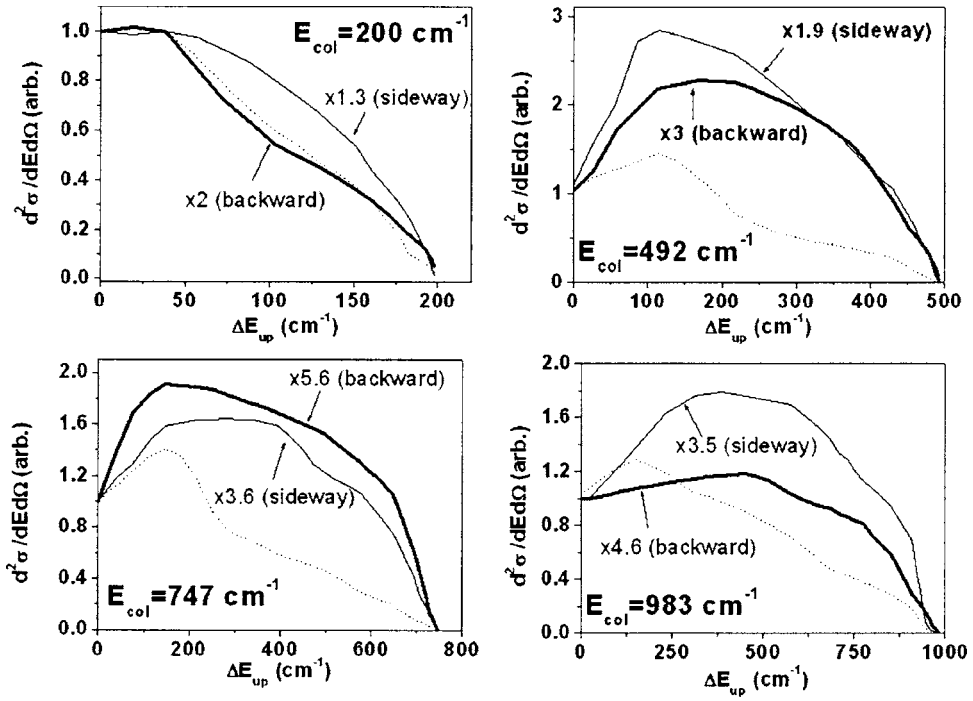


FIG. 3. *T-V/R* energy-transfer probability distribution functions at various scattering angles. Dotted line: forward scattering $(50<\theta<60$ for collision energies of 200 and 492 $cm^{-1}$ and $40<\theta<50$ for collision energies of 747 and 983 $cm^{-1}$), thin solid line: sideway scattering $(80<\theta<100)$, and thick solid line: backward scattering $(160<\theta<180)$.

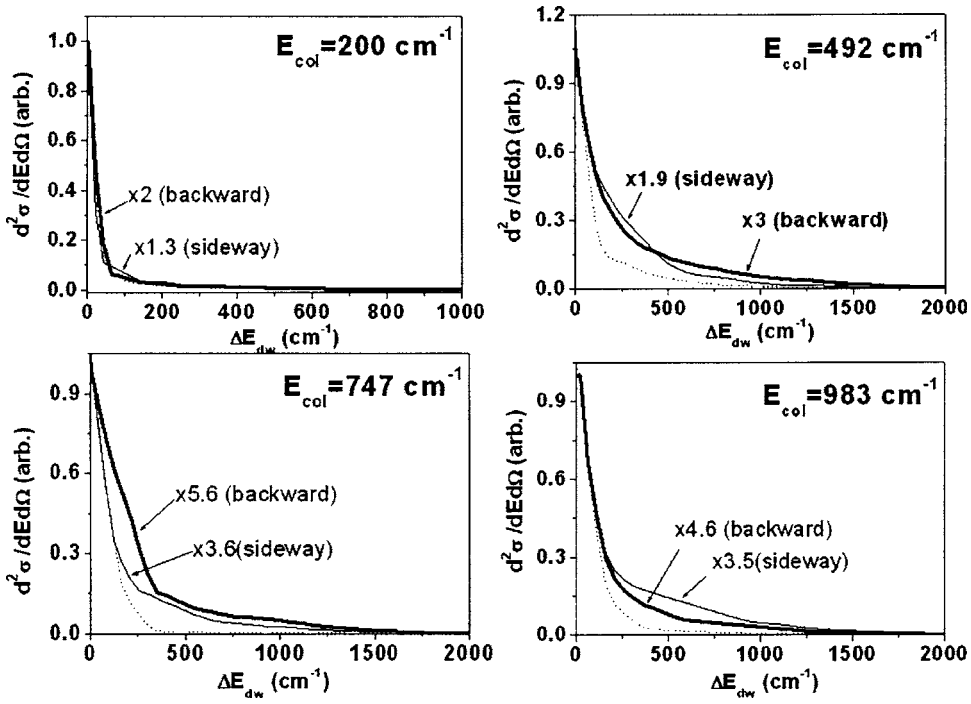


FIG. 4. *V-T* energy-transfer probability distribution functions at various scattering angles. Dotted line: forward scattering ($50<\theta<60$ for collision energies of 200 and 492 $cm^{-1}$ and $40<\theta<50$ for collision energies of 747 and 983 $cm^{-1}$), thin solid line: sideway scattering ($80<\theta<100$), and thick solid line: backward scattering ($160<\theta<180$).

There is a tail in the high-energy region for both sideway and backward scatterings and transferred energies as large as 500–2000 $cm^{-1}$ can be observed. For energy up collisions, the respective shapes for forward, sideway, and backward scatterings all differ.

The importance of the large energy transfer in the backward direction can be seen from differential cross section at large energy transfer. Figure 5 shows the differential cross section which the amount of energy transfer is larger than 500 or 1500 $cm^{-1}$. It is clear that the differential cross sections in the backward direction have large values than that in the other directions for large energy transfer.

In principle, the total energy transfer probability distribution function can be obtained directly from the summation of the probability distribution functions at various scattering angles. Since the image has large intensity in the forward direction and a large portion of the image at forward direction was obscured by the stainless steel pin, we cannot obtain the total energy transfer probability distribution function.

## IV. DISCUSSION

Although they are small differences, the collisions between highly vibrationally excited azulene and Ar in general

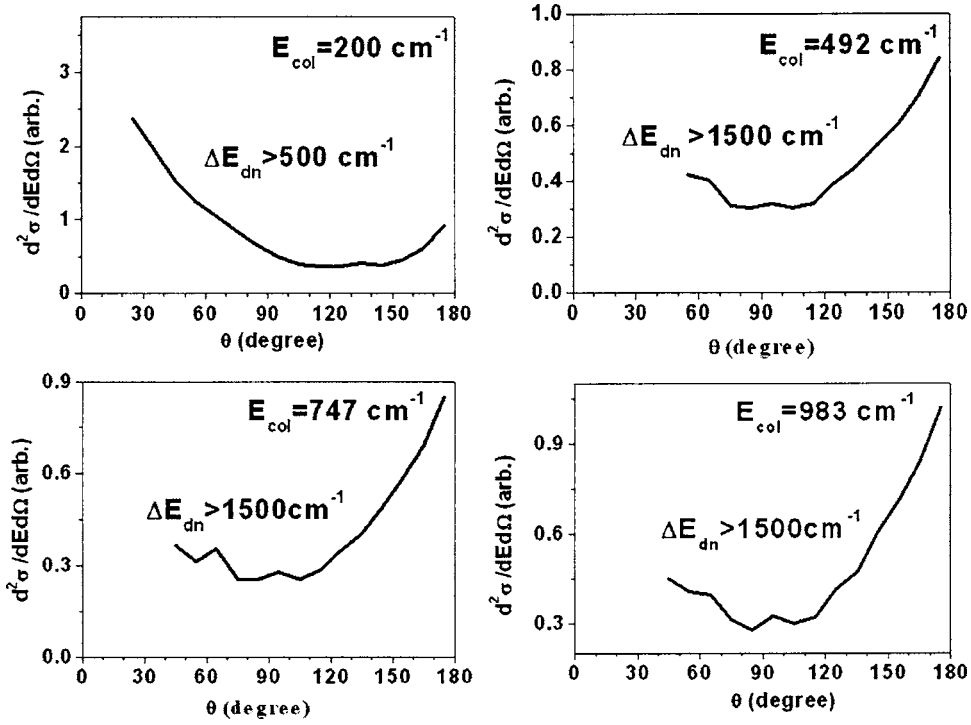


FIG. 5. Differential cross section for large energy transfer.

are similar to the collisions between highly vibrationally excited azulene and Kr. The similarities and differences are summarized as follows.

We observed a strong forward scattering peak for both $\Delta E_{up}$ and $\Delta E_{dn}$ collisions at all different collision energies in Az–Ar collisions. However, there is a weak backward scattering peak at the lowest collision energy. It indicates the formation of a short-lived azulene–Ar complex. In the collisions between azulene and Kr, we also observed strong forward scattering peaks, but the intensities of backward peaks found in Az–Kr collisions are much larger and they were observed at collision energy up to 780 $cm^{-1}$. The relatively easy formation of complex between Az–Kr can be rationalized from the larger depth of van der Waals potential well. Although Ar (or Kr) stays close to the highly vibrationally excited azulene during the period of complex, instead of energy transfer from vibration to translation, the formation of complex only results in the small amount of energy transfer from translation to vibration/rotation.

For both Az–Ar and Az–Kr, the $\Delta E_{up}$ maximum approaches the collision energy (the maximum available energy), indicating that translational energy can be transferred almost entirely to vibrational/rotational energy. On the other hand, only a small amount of available vibrational energy is converted to translational energy in both systems. The maximum vibrational energy released to translational energy can be determined up to 2000 $cm^{-1}$ according to the signal-to-noise ratio $S/N=1$. This is much smaller than the maximum vibrational energy released to translational energy ($\sim$5000 $cm^{-1}$) in Az–Kr. It is likely similar to the mass effect in the energy transfer which has been observed in the average energy transfer in the collisions between Az–Ar and Az–Kr in thermal system.[2]

Although we did not publish the relative cross sections between *T-V/R* and *V-T* for Az–Kr collisions in previous paper, the changes with collision energy were found to be similar to that in Az–Ar collisions, i.e., the total cross section of *T-V/R* becomes small at low collision energy. This can be understood from the fact that at very small collision energy, almost no translational energy can be transferred to vibration/rotation. Collisions only end up as vibration to translation energy transfer. However, it is interesting to notice that *T-V/R* cross section becomes much larger than the *V-T* cross section at large collision energy. One of the possible explanations is that most of the translational energy is transferred to rotational energy. This is because the energy transfer between translation and rotation is efficient, and azulene in the molecular beam is initially rotationally cold.

Finally, one of the most important similarities between Az–Ar and Az–Kr is that most of the large energy transfer, such as supercollisions, occurs in the backward direction at large collision energies. It indicates the small impact parameters and large collision energy are the necessary conditions for large energy transfer. However, sideway scatterings start to play important role in large energy transfer in Az–Ar collisions at relatively small collision energy compared to Az–Kr collisions.

## ACKNOWLEDGMENT

The work was supported by the National Science Council (NSC), Taiwan under Contract No. NSC 94-2113-M-001-036.

[1] D. C. Tardy and B. S. Rabinovitch, Chem. Rev. (Washington, D.C.) **77**, 369 (1977).
[2] I. Oref and D. C. Tardy, Chem. Rev. (Washington, D.C.) **90**, 1407 (1990).
[3] J. R. Barker, L. M. Yoder, and K. D. King, J. Phys. Chem. A **105**, 796 (2001).
[4] M. J. Rossi and J. R. Barker, J. Chem. Phys. **88**, 6219 (1982).
[5] M. J. Rossi, J. R. Pladziewicz, and J. R. Barker, J. Chem. Phys. **78**, 6695 (1983).
[6] J. M. Zellweger, T. C. Brown, and J. R. Barker, J. Phys. Chem. **90**, 461 (1986).
[7] J. M. Zellweger, T. C. Brown, and J. R. Barker, J. Chem. Phys. **83**, 6251 (1985).
[8] J. M. Zellweger, T. C. Brown, and J. R. Barker, J. Chem. Phys. **83**, 6261 (1985).
[9] J. Shi, D. Bernfeld, and J. R. Barker, J. Chem. Phys. **88**, 6211 (1988).
[10] J. Shi and J. R. Barker, J. Chem. Phys. **88**, 6219 (1988).
[11] G. V. Hartland, D. Qin, and H. L. Dai, J. Chem. Phys. **100**, 7832 (1994).
[12] G. V. Hartland, D. Qin, and H. L. Dai, J. Chem. Phys. **101**, 8554 (1994).
[13] H. Hipper, L. Lindemann, and J. Troe, J. Chem. Phys. **83**, 3906 (1985).
[14] H. Hippler, J. Troe, and H. J. Wendelken, Chem. Phys. Lett. **84**, 257 (1984).
[15] H. Hippler, J. Troe, and H. J. Wendelken, J. Chem. Phys. **78**, 5351 (1983).
[16] M. Heymann, H. Hippler, and J. Troe, J. Chem. Phys. **80**, 1853 (1984).
[17] H. Hilpper, Ber. Bunsenges. Phys. Chem. **89**, 303 (1985).
[18] J. E. Dove, H. Hippler, and J. Troe, J. Chem. Phys. **82**, 1907 (1985).
[19] L. Brouwer, H. Hippler, L. Lindemann, and J. Troe, J. Phys. Chem. **89**, 4608 (1985).
[20] C. J. Cobos, H. Hippler, and J. Troe, J. Phys. Chem. **89**, 1778 (1985).
[21] J. E. Dove, H. Hippler, J. Plach, and J. Troe, J. Chem. Phys. **81**, 1209 (1984).
[22] B. Herzog, H. Hippler, L. Kang, and J. Troe, Chem. Phys. Lett. **120**, 124 (1985).
[23] N. Nakashima and Y. Yoshihara, J. Chem. Phys. **79**, 2727 (1983).
[24] T. Ichimura, Y. Mori, N. Nakashima, and Y. Yoshihara, J. Chem. Phys. **83**, 117 (1985).
[25] T. Ichimura, M. Takahashi, and Y. Mori, Chem. Phys. **114**, 111 (1987).
[26] E. T. Sevy, S. M. Rubin, Z. Lin, and G. W. Flynn, J. Chem. Phys. **113**, 4912 (2000).
[27] C. A. Michaels, A. S. Mullin, J. Park, J. Z. Chou, and G. W. Flynn, J. Chem. Phys. **108**, 2744 (1998).
[28] C. A. Michaels, Z. Lin, A. S. Mullin, H. C. Tapalian, and G. W. Flynn, J. Chem. Phys. **106**, 7055 (1997).
[29] C. A. Michaels and G. W. Flynn, J. Chem. Phys. **106**, 3558 (1997).
[30] M. S. Elioff, M. Fang, and A. S. Mullin, J. Chem. Phys. **117**, 6880 (2002).
[31] J. Park, L. Shum, A. S. Lemoff, K. Werner, and A. S. Mullin, J. Chem. Phys. **117**, 5221 (2002).
[32] J. Park, Z. M. Li, A. S. Lemoff, C. Rossi, M. S. Elioff, and A. S. Mullin, J. Phys. Chem. **106**, 3642 (2002).
[33] M. S. Elioff and A. S. Mullin, J. Chem. Phys. **115**, 6990 (2001).
[34] M. C. Wall and A. S. Mullin, J. Chem. Phys. **108**, 9658 (1998).
[35] S. Hassoon, I. Oref, and C. Steel, J. Chem. Phys. **89**, 1743 (1988).
[36] L. M. Morgulis, S. S. Sapers, C. Steel, and I. Oref, J. Chem. Phys. **90**, 923 (1989).
[37] A. Pashutzki and I. Oref, J. Phys. Chem. **92**, 178 (1988).
[38] U. Hold, T. Lenzer, K. Luther, K. Reihs, and A. C. Symonds, J. Chem. Phys. **112**, 4076 (2000).
[39] T. Lenzer, K. Luther, K. Reihs, and A. C. Symonds, J. Chem. Phys. **112**, 4090 (2000).
[40] U. Hold, T. Lenzer, K. Luther, and A. C. Symonds, J. Chem. Phys. **119**, 11192 (2003).
[41] H. C. Hsu, J. J. Lyu, C. L. Liu, C. L. Huang, and C. K. Ni, J. Chem. Phys. **124**, 054301 (2006).
[42] C. L. Liu, H. C. Hsu, J. J. Lyu, and C. K. Ni, J. Chem. Phys. **123**, 131102 (2005).

[43] C. L. Liu, H. C. Hsu, J. J. Lyu, and C. K. Ni, J. Chem. Phys. **124**, 054301 (2006).
[44] V. Bernshtein and I. Oref, J. Chem. Phys. **125**, 133105 (2006).
[45] V. Bernshtein, I. Oref, C.-L. Liu, H. C. Hsu, and C.-K. Ni, Chem. Phys. Lett. **429**, 317 (2006).
[46] M. Fuji, T. Ebata, N. Mikami, and M. Ito, Chem. Phys. **77**, 191 (1983).
[47] Y. A. Dyakov, C. K. Ni, S. H. Lin, Y. T. Lee, and A. M. Mebel, J. Phys. Chem. A **109**, 8774 (2005).
[48] J. J. Lin, J. Zhou, W. Shiu, and K. Liu, Rev. Sci. Instrum. **74**, 2495 (2003).
[49] C. L. Liu, H. C. Hsu, and C. K. Ni, Phys. Chem. Chem. Phys. **7**, 2151 (2005).